

KECK/DEIMOS SPECTROSCOPY OF A GALEX UV SELECTED SAMPLE FROM THE MEDIUM IMAGING SURVEY *

RYAN P. MALLERY¹, R. MICHAEL RICH¹, SAMIR SALIM¹, TODD SMALL², STEPHANE CHARLOT^{3,4}, MARK SEIBERT², TED WYDER², TOM A. BARLOW², KARL FORSTER², PETER G. FRIEDMAN², D. CHRISTOPHER MARTIN², PATRICK MORRISSEY², SUSAN G. NEFF⁵, DAVID SCHIMINOVICH⁶, LUCIANA BIANCHI⁷, JOSE DONAS⁸, TIMOTHY M. HECKMAN⁹, YOUNG-WOOK LEE¹⁰, BARRY F. MADORE¹¹, BRUNO MILLIARD⁸, ALEX S. SZALAY⁹, BARRY Y. WELSH¹², SUK YOUNG YI¹⁰

Draft version August 21, 2021

ABSTRACT

We report results from a pilot program to obtain spectroscopy for objects detected in the *Galaxy Evolution Explorer* (GALEX) Medium Imaging Survey (MIS). Our study examines the properties of galaxies detected by GALEX fainter than the Sloan Digital Sky Survey (SDSS) spectroscopic survey. This is the first study to extend the techniques of (Salim et al. 2005) to estimate stellar masses, star formation rates (SFR) and the *b* (star formation history) parameter for star-forming galaxies out to $z \sim 0.7$. We obtain redshifts for 50 GALEX MIS sources reaching $NUV = 23.9$ (AB mag), having counterparts in the SDSS Data Release 4 (DR4). Of our sample, 43 are starforming galaxies with $z < 0.7$, 3 have emission line ratios indicative of AGN with $z < 0.7$, and 4 objects with $z > 1$ are QSOs, 3 of which are not previously cataloged. We compare our sample to a much larger sample of $\sim 50,000$ matched GALEX/SDSS galaxies with SDSS spectroscopy; while our survey is shallow, the optical counterparts to our sources reach ~ 3 magnitudes fainter in SDSS *r* than the SDSS spectroscopic sample. We use emission line diagnostics for the galaxies to determine that the sample contains mostly star-forming galaxies. The galaxies in the sample populate the blue sequence in the $NUV - r$ vs M_r color-magnitude diagram. The derived stellar masses of the galaxies range from 10^8 to $10^{11} M_{\odot}$ and derived SFRs are between 10^{-1} and $10^2 M_{\odot} yr^{-1}$. Our sample has SFRs, luminosities, and velocity dispersions that are similar to the samples of faint compact blue galaxies studied previously in the same redshift range by Koo et al (1995), Guzmán et al. (1996), & Phillips et al. (1997). However, our sample is ~ 2 mag fainter in surface brightness than the compact blue galaxies. We find that the star-formation histories for a majority of the galaxies are consistent with a recent starburst within the last 100 Myr.

Subject headings: galaxies: active galaxies:redshifts galaxies: starburst ultraviolet: galaxies

*SOME OF THE DATA PRESENTED HEREIN WERE OBTAINED AT THE W.M. KECK OBSERVATORY, WHICH IS OPERATED AS A SCIENTIFIC PARTNERSHIP AMONG THE CALIFORNIA INSTITUTE OF TECHNOLOGY, THE UNIVERSITY OF CALIFORNIA AND THE NATIONAL AERONAUTICS AND SPACE ADMINISTRATION. THE OBSERVATORY WAS MADE POSSIBLE BY THE GENEROUS FINANCIAL SUPPORT OF THE W.M. KECK FOUNDATION.

¹ Department of Physics and Astronomy, University of California, Los Angeles, CA 90095-1562

² California Institute of Technology, MC 405-47, 1200 East California Boulevard, Pasadena, CA 91125

³ Max-Planck Institut für Astrophysik, D-85748 Garching, Germany

⁴ Institut d'Astrophysique de Paris, CNRS, 98 bis boulevard Arago, F-75014 Paris, France

⁵ Laboratory for Astronomy and Solar Physics, NASA Goddard Space Flight Center, Greenbelt, MD 20771

⁶ Department of Astronomy, Columbia University, New York, NY 10027

⁷ Center for Astrophysical Sciences, The Johns Hopkins University, 3400 N. Charles St., Baltimore, MD 21218

⁸ Laboratoire d'Astrophysique de Marseille, BP 8, Traverse du Siphon, 13376 Marseille Cedex 12, France

⁹ Department of Physics and Astronomy, The Johns Hopkins University, Homewood Campus, Baltimore, MD 21218

¹⁰ Center for Space Astrophysics, Yonsei University, Seoul 120-749, Korea

¹¹ Space Sciences Laboratory, University of California at Berkeley, 601 Campbell Hall, Berkeley, CA 94720

¹² Observatories of the Carnegie Institution of Washington, 813 Santa Barbara St., Pasadena, CA 91101

¹³ Space Sciences Laboratory, University of California at Berkeley, 601 Campbell Hall, Berkeley, CA 94720

1. INTRODUCTION

Following the successful launch and early operations of the *Galaxy Evolution Explorer* satellite in 2003, we decided to undertake an initial spectroscopic assay of sources detected by GALEX using the DEIMOS multi-object spectrograph (Faber et al. 2003) on the Keck II telescope. Although GALEX data have been matched to relatively deep optical surveys (Schiminovich et al. 2005) our study is the first to extend the modeling technique of Salim et al. (2005) from $z = 0.25$ to $z \sim 0.5$.

The power of the GALEX Medium Imaging Survey to select interesting objects is noteworthy. We recall that the MIS observations are 1500 sec in duration, imaging FUV and NUV simultaneously (Martin et al. (2005a) & Morrissey et al. (2005)). The GALEX satellite has investigated the ultraviolet universe to $z \sim 1$ with the goal of determining among other things, the star formation rate (SFR) of galaxies in the local universe, $z \lesssim 0.25$ (Salim et al. 2005; Martin et al. 2005b; Wyder et al. 2005; Treyer et al. 2005) and the evolution of the global star formation density out to $z \sim 1$ (Schiminovich et al. 2005). The ultimate goal of such work along with other surveys and observations of galaxies at similar and higher redshifts is to constrain the baryonic physics of galaxy formation and evolution. Questions still remain as to how the SFR depends on different factors such as envi-

ronment, mass, morphology etc. (Martin et al. 2005a). Previous work deriving SFRs with a UV-selected sample was carried out by Sullivan et al. (2000) who derive SFRs both from UV luminosities at 2000\AA and $H\alpha$ luminosities from optical spectra for a sample of galaxies at redshifts of $0 < z < 0.4$ detected in the UV by the balloon-borne telescope FOCA (Milliard, B. et al. 1992). Estimates of local star formation rates before this were only possible through either optical emission line luminosities of the recombination lines of Hydrogen, mostly $H\alpha$, and $[\text{OII}]\lambda 3727$ or the far infrared luminosity from $10\text{-}100\mu\text{m}$ (Kennicutt 1998).

In this paper we present the observations and results from the pilot program for a sample of objects detected by *GALEX* and SDSS with spectra obtained from the DEIMOS spectrograph at the Keck II telescope. The analysis of this sample is enhanced greatly by the techniques of Salim et al. (2005) that have been expanded to include the derivation of galaxy physical parameters such as stellar mass, from *GALEX* + SDSS photometry and redshifts. The main goal of this paper is to characterize the galaxies detected by *GALEX* that are fainter than SDSS Spectroscopic Galaxy Sample, in terms of mass, SFR, and UV-optical color. We are predominantly (about two-thirds of the sample) seeing the faint blue galaxy population (Ellis 1997) and are also sensitive to QSOs. While *GALEX* observations have been undertaken in many deep fields with much higher median redshifts (Schiminovich et al. 2005) we have the advantage in this sample of obtaining spectroscopy with Keck/DEIMOS, which gives wavelength coverage sufficient to derive some detailed physical parameters from the spectra. In §2 we describe the Sample and the photometric and spectroscopic data. Redshift and emission line flux measurements from the spectroscopy are presented in §3. The distributions of UV color, UV-optical color, and the SDSS r magnitude for the sample are described in §4. The derived galaxy parameters from SED fits are described in §5. We give a discussion and summary of our findings in §6 and 7. Throughout this paper we assume $H_0=70 \text{ km s}^{-1} \text{ Mpc}^{-1}$, $\Omega_m=0.3$, and $\Omega_\Lambda=0.7$.

2. SAMPLE AND OBSERVATIONS

2.1. *GALEX*/SDSS Data

GALEX is a NASA Small Explorer Mission aimed to survey the UV emission from Galactic and extragalactic sources from 700km circular orbit (Martin et al. 2005a; Morrissey et al. 2005). *GALEX* images the sky simultaneously in two bands, the far-UV (FUV $1344\text{-}1786\text{\AA}$) and the near-UV (NUV $1771\text{-}2831\text{\AA}$). Each *GALEX* circular field is 1.25 deg. in diameter. We use FUV and NUV magnitudes and magnitude errors derived in elliptical apertures¹⁴. The photometry is taken from the *GALEX* Internal Release 1.1 (IR1.1). The *GALEX* MIS photometry for tile number 10273 has a limiting magnitude, $m_{lim}(\text{AB})=23$.

We use optical photometry for our objects obtained from SDSS Data Release 4 (DR4) (Abazajian et al. 2004). The SDSS photometric data are taken with the 2.5m telescope at Apache Point Observatory. Imag-

ing is obtained in *ugriz* bands (Fukugita et al. 1996; Smith et al. 2002). The imaging data are photometrically (Hogg et al. 2001) and astrometrically (Pier et al. 2003) calibrated. An overview of the SDSS data pipelines and products can be found in Stoughton et al. (2002).

2.2. Sample

Our sample is derived from objects with detections in the *GALEX* Medium Imaging Survey (MIS) tile 10273, centered at a right ascension/declination of $17^{\text{h}}40^{\text{m}}32.07^{\text{s}} / 57^{\circ}10'45.15''$.

The *GALEX* field being much larger than the DEIMOS slit mask, we selected objects from the *GALEX* field to populate two DEIMOS slit masks. The two DEIMOS fields were initially chosen to maximize the number of MIS objects with optical counterparts in the SDSS classified as galaxies with $FUV-NUV < 0$ photometry from an early version of the *GALEX* data reduction pipeline. The number of galaxies matching this criteria was much smaller than the number of available slits, and so to take full advantage of the DEIMOS field of view, the slits were populated by any galaxy detected by both *GALEX* and SDSS. In addition, the remainder of available slits in both fields was populated with blue stellar-like objects (QSOs and white dwarfs), main sequence outlier stars ($u-g < 1$ or $g-r < 0$), and bright alignment stars. The first DEIMOS field contains 26 objects classified as galaxies in SDSS, and 10 blue stellar objects and main sequence outlier stars. The second DEIMOS field contains 19 objects classified as galaxies in SDSS, and 9 blue stellar objects and main sequence outlier stars.

2.3. Spectroscopic observations

The spectroscopic data were obtained at the Keck II telescope with the DEIMOS multi-object spectrometer on October 1, 2003 (Faber et al. 2003). Spectra were obtained using two slit masks, for a total 64 spectra. The $830 \text{ grooves mm}^{-1}$ grating was used with a slit width of $0''.73$ giving a resolution of $\sim 2.5\text{\AA}$ FWHM. The signal-to-noise ratio obtained over the continuum of each spectrum varied between sources from 1 to ~ 20 , depending on the brightness of the source. The integration time for both slit masks was 30 minutes. Flux calibration of the spectra was not performed as no flux standards were observed. The spectra cover a wavelength range of $\sim 5000 - 9000\text{\AA}$. Figure 1 shows a panel of several one dimensional spectra for star-forming galaxies in the sample at a range of redshifts, plotted in the rest wavelength, and Figure 2 shows the spectra for objects with measured $z > 1$.

3. REDSHIFT DETERMINATION AND MEASUREMENT OF EMISSION LINES

In all, we measured 50 redshifts, 45 for sources classified as galaxies in SDSS and 5 for sources classified as stars in SDSS. Of those five, three are QSO's at $z > 1$ and the other two are star-forming galaxies. The remaining 14 of the sources classified as stars by the SDSS have stellar spectra. The redshifts for objects with detected emission lines were measured by eye. For objects with $z < 1$, multiple emission lines were detected including either $H\alpha$ and/or $H\beta$ and $[\text{OII}]\lambda 3727$, $[\text{OIII}]\lambda 4959$, $[\text{OIII}]\lambda 5007$, $[\text{NII}]\lambda 6584$, $[\text{SII}]\lambda 6717$, and $[\text{SII}]\lambda 6731$. For

¹⁴ *GALEX* source detection and measurement is obtained from SExtractor (Bertin, & Arnouts 1996)

all objects where the doublet [OII] λ 3727 was detected, H α was redshifted beyond the wavelength range of the detector. For one source, at $z=1.028$, we detected two features that we assigned as [OII] λ 3727 and MgII λ 2800 emission. For the other three sources with $z > 1$ we find only 1 feature that we identify as MgII λ 2800, based on the width of the line and the absence of other features in the spectrum. Figure 3 shows the redshift distribution of the sample. The mean redshift of the sample is $z_{mean} = 0.421$. Two of the sources in the DEIMOS sample have corresponding SDSS spectra. The redshifts obtained for these two objects agree with the SDSS redshifts. One of the objects with SDSS spectra is the QSO at $z = 1.028$ and the other is a galaxy at $z = 0.176$. Both the DEIMOS spectra and the SDSS spectra for the latter object have significant detections of only H α and [NII] λ 6584.

We measure spectral emission line fluxes and equivalent widths for [OII] λ 3727, H β , [OIII] λ 4959, [OIII] λ 5007, H α , [NII] λ 6584, [SII] λ 6717, and [SII] λ 6731. Fluxes, equivalent widths and errors for the emission lines were measured in IDL using the MPFIT function. The continuum of each spectrum was first fit by a polynomial, then the emission lines were simultaneously fit with gaussians. Table 1 lists the objects, their equivalent widths and flux ratios of [OIII] λ 5007/H β and [NII] λ 6584/H α for objects with a 3σ measurement of at least one of the above lines. We did not perform a reddening correction to the fluxes, since the standard procedure requires either detections of both H α and H β or a measurement of the radio continuum (Osterbrock 1989). The effect of this on the flux ratios of [OIII] λ 5007/H β and [NII] λ 6584/H α is thought to be negligible due to the small wavelength separation of the emission lines. In the DEIMOS sample we only have detections of both H α and H β for 18 objects, all at $z < 0.3$, and chose for consistency not to perform corrections on any of the spectra. We note that the foreground Galactic extinction, E(B-V), calculated from the dust maps of D.J. Schlegel, D.P. Finkbeiner, & M. Davis (1998) is $\sim .05$ magnitudes for the field.

Fourteen objects have measured fluxes of H β , [OIII] λ 5007, H α , and [NII] λ 6584. Figure 4 shows the emission line diagnostic of Baldwin, Phillips, & Terlevich (1981) used to distinguish star-forming galaxies and Type II AGN. The solid curve is the boundary between star-forming galaxies and AGN determined through modeling of starburst galaxy spectra by Kewley et al. (2001). A star forming galaxy with only $\sim 20\%$ of the optical emission line flux due to an AGN would lie above the star-forming/AGN boundary (Kewley et al. 2001). The dashed curve is the more stringent demarcation used by Kauffmann et al. (2003) to distinguish between AGN and star-forming galaxies in SDSS. The shaded histogram shows the distribution of emission line ratios for a sample of 51,000 SDSS/GALEX objects (see §4). The curve of Kauffmann et al. (2003) distinguishes between the two different sources of emission line flux in this large sample with the AGN occupying the parameter space to the right of the distribution of star-forming galaxies. In the DEIMOS sample only three galaxies of the fourteen have emission line flux ratios above this curve, implying that some portion of the flux is due to an AGN, though

it is still within the errors that the emission line flux for two of these objects results entirely from star-forming regions inside the host galaxies. Objects can also be AGN if $\log [\text{OIII}]/\text{H}\beta > 1$ or $\log [\text{NII}]/\text{H}\alpha > 0.3$. Another 13 objects also have only detections of H β and [OIII] λ 5007. Of the thirteen, one has a flux ratio of $\log [\text{OIII}]/\text{H}\beta > 1$, indicative of an AGN. Sullivan et al. (2000) find a similar ratio of galaxies classified as star-forming/AGN from examination of emission lines in their sample of UV selected galaxies.

4. MAGNITUDE AND COLOR DISTRIBUTION

The DEIMOS sample is ~ 3 magnitudes deeper in r than the SDSS spectroscopic sample. Figure 5 shows a histogram of the SDSS r magnitudes for the sample plotted with the SDSS r magnitude for GALEX MIS sources in IR1.1 with matches in the SDSS DR2 spectroscopic sample. The IR1.1/DR2 sample consists of $\sim 51,000$ galaxies at redshifts $0.005 < z < 0.25$ with derived star-formation histories (SFHs) by SED fitting (see §5). The IR1.1/DR2 histogram is normalized to the size of the DEIMOS galaxy sample. The IR1.1/DR2 sample is mostly bounded in r by the SDSS spectroscopic survey limits, $r < 17.7$ (Strauss et al. 2002).

Using the redshifts determined for the DEIMOS sample we calculate the absolute r magnitude, M_r , of galaxies in the sample, k-corrected to the mean redshift of the IR1.1/DR2 sample, $z = 0.1$. K-corrections for all band-passes were calculated using the publicly available code of Blanton et al. (2003) version 4_1_4. In Figure 6 we construct a color magnitude diagram (CMD) of $NUV - r$ versus M_r . We overplot our sample onto the IR1.1/DR2 sample, plotted as a shaded contour plot. In the figure the diamond symbols correspond to DEIMOS objects with spectroscopically measured redshifts at $z < 0.25$, and the crosses correspond to objects with spectroscopically measured redshifts at $z > 0.25$. The contours enclose 40% and 80% of the objects in the IR1.1/DR2 sample.

The CMD of the IR1.1/DR2 sample clearly shows the bimodality of galaxies seen by GALEX in the nearby universe, $z < 0.25$, with distribution peaks at blue $NUV - r$ colors of ~ 3 and at red $NUV - r$ colors of ~ 6 (Wyder et al. 2005). We henceforth call these the blue and red sequences. The galaxies in the blue sequence are generally late-type in morphology and have spectra with emission line-ratios indicative of star-formation (Salim et al. 2005; Brinchmann et al. 2004), while the galaxies in the red sequence typically have absorption line spectra and lower star-formation rates than blue sequence galaxies. The majority of the objects in the DEIMOS sample lie in the region of the diagram occupied by blue star-forming galaxies in the IR1.1/DR2 sample, mostly along the blue edge of the distribution, with only one having a $NUV - r$ color greater than 4. The spectrum for this object, at $z = 0.077$, is shown in Figure 1. The spectrum shows absorption features: NaD, and MgIb, but also shows weak emission features of H α , [NII] λ 6584, and [SII] λ 6717,6731.

In the bottom-left panel of Figure 7 we again plot the color magnitude diagram for the sample, highlighting the objects with FUV detections (filled circles). The other 3 panels of this figure show the UV color distribution for the 24 galaxies in the DEIMOS sample with FUV

detections. Plotted for reference are galaxies from the IR1.1/DR2 sample with FUV detections shown as the shaded contour plots or shaded histogram in the respective panels. Besides the 3 galaxies in the DEIMOS sample with $FUV - NUV < 0$ the UV color for this sample shows a similar distribution with the IR1.1/DR2 sample. In the FUV CMD the objects with $M_r < 20$ show a range of UV color not seen in the local blue sequence galaxies of similar optical luminosity. Both figures 6 and 7 show that this sample probes the type of galaxies that one obtains when looking at objects detected by *GALEX* several magnitudes deeper than the SDSS spectroscopic limit.

5. DERIVED GALAXY PARAMETERS

We derive the following galaxy parameters according to the approach of Salim et al. (2005): the V-band dust attenuations, A_V in magnitudes, stellar metallicity Z , the current star formation rate, SFR, averaged over the past 100 Myr in $M_\odot \text{ yr}^{-1}$, the present-day stellar mass, M_* , of the galaxy in M_\odot , the fraction of stellar mass formed in bursts over the last 100 Myr, F_{burst} , and the Scalo (1986) b parameter, defined as the ratio of the current SFR to the past time-averaged SFR (averaged over the estimated age, not Hubble time). The galaxy parameters are derived from model libraries of galaxies at redshifts between 0.1 and 1.6 at redshift increments of 0.1 for the DEIMOS sample, and at redshifts of 0.05, 0.1, 0.15, 0.2, and 0.25 for the IR1.1/DR2 sample. Each library consists of up to $\sim 10^5$ models. Each model is parameterized according to galaxy age, optical depth, star formation history (SFH), and metallicity. The SFH of each model is parameterized according to Kauffmann et al. (2003), with an underlying, continuous, exponentially declining SFR upon which bursts of star formation, random in time and amplitude, are superimposed. Dust attenuation in each model is parameterized using the prescription of Charlot & Fall (2000) using an effective V-band optical depth τ_V and absorption curve, $\tau \propto \lambda^{0.7}$ resulting from both giant molecular clouds and the diffuse ISM, with the fraction μ of τ_V contributed only by the diffuse ISM. The V-band optical depth from giant molecular clouds is taken to only affect stars younger than 10 Myr. A description of the prior distributions of the model parameters is discussed in Salim et al. (2005).

Spectral energy distributions (SEDs) are created for each galaxy in the library using the population synthesis code of Bruzual & Charlot (2003). The model SEDs are convolved with the *GALEX* and SDSS filter response curves. Statistical estimates of physical galaxy parameters are derived by comparing the observed 7 band *GALEX*/SDSS fluxes of each galaxy to all the convolved model SEDs in the nearest redshift library. Probability density functions (PDFs) for each physical parameter are created by assigning weights to the parameters. The χ^2 goodness of fit of the model determines the weight ($\propto \exp[-\chi^2/2]$) that is assigned to the parameters of that model. The median (or most typical parameter value) of the PDF is taken as the estimate of the galaxy parameter.

We perform SED fits for galaxies not identified as QSOs. In Table 2 we list the galaxies, their redshifts, $NUV - r$ non k-corrected colors, and their derived parameters. The parameters derived from the SED fits are

not used unless the reduced χ^2 fit of at least one model is below 10. Only two of the 46 galaxies do not meet this criterion. Figures 8 and 9 show the derived parameters for the DEIMOS sample of galaxies overplotted on the IR1.1/DR2 sample plotted as shaded contour plots. The contours are labeled and encompass 52%, 84%, and 97% of the data. The diamonds as before are objects with $z < 0.25$, and the crosses are objects with $z > 0.25$. The objects span the range of derived parameters of the IR1.1/DR2 sample for Z , and A_V .

The derived metallicities, $Z = [Fe/H]$, for the sample are not very well constrained. The typical error, 1/4 of the difference between the 97.5 percentile and the 2.5 percentile of the PDF, of the derived metallicities are $\pm 43\% Z_\odot$. The derived M_* range from 10^8 to $10^{11} M_\odot$ with an average error of $\sim \pm 0.2\text{dex}$, but the majority of the M_* are at or below $10^{10} M_\odot$, about an order of magnitude below the mean of the IR1.1/DR2 sample. The derived SFRs lie between 10^{-1} and $10^2 M_\odot \text{ yr}^{-1}$, with five galaxies having derived SFRs greater than $10 M_\odot \text{ yr}^{-1}$. The average error on the derived SFRs is typically $\pm 0.3\text{dex}$. Comparing the SFRs between galaxies with similar $NUV - r$ color or M_* , the galaxies at $z > 0.25$ have SFRs about an order of magnitude greater than the galaxies at $z < 0.25$. This is mostly a selection effect since the more distant galaxies are also more luminous on average. A comparison of these SED derived SFRs with $H\alpha$ derived SFRs cannot be performed since the spectra are not flux calibrated and many lack $H\alpha$. The range of SFRs we find for this sample is similar to the range of SFRs for local UV galaxies found by Sullivan et al. (2000) derived both from $H\alpha$ luminosity and from the UV luminosity, but is an order of magnitude larger than the SFRs found by Kobulnicky & Kewley (2004) in their sample of Goods-North Treasury Keck Redshift Survey galaxies at $0.4 < z < .9$ when compared to galaxies in the DEIMOS sample with similar redshifts.

We find that the galaxies are largely starbursts with $\log b \sim -0.1$. This is shown in Figure 10. The distribution of $\log b$ for objects in the DEIMOS sample with SED fits are plotted with the distribution for the IR1.1/DR2 sample normalized to the number of objects in the DEIMOS sample with SED fits. The DEIMOS sample shows a highly peaked value of $\log b$ compared to the IR1.1/DR2 sample which has two small peaks near $\log b \sim -3$ and ~ -1 , showing that most of these galaxies currently have less star-formation now than in the past. The value $\log b \sim -0.1$ that describes most of the galaxies in the DEIMOS sample indicates that while these galaxies have less star formation than in the past, they are currently or have recently gone through a burst of star-formation. Two of the galaxies have $\log b > 0$ indicating that these galaxies are going through major starbursts in their histories. From a statistical standpoint, the SED fits reveal with a 95% reliability that at least three galaxies have not had a burst of starformation in the last 100 Myr. Half of the galaxies in the sample could have formed as much as $\sim 10\%$ of their stellar mass in a burst within the last 100 Myr, 10 could have formed up to $\sim 25\%$ and five of the less massive systems could have had up to $\sim 50\%$ of their stellar mass form in bursts within the last 100Myr.

6. DISCUSSION

In the plot of $NUV - r$ vs M_r our sample lies along a “blue sequence” of star forming galaxies and they have among the bluest colors for star forming galaxies in the local Universe found by *GALEX* and SDSS. While all the galaxies show blue $NUV - r$ color this is not a homogenous sample. Fifteen of the galaxies show disk structure in the SDSS images. The remaining two-thirds of the sample fit into the heterogeneous class of faint blue galaxies at intermediate redshifts previously studied by Koo et al (1995); Guzmán et al. (1996, 1998); Phillips et al. (1997) and Guzmán et al. (1997) in the Hubble Deep Field and adjoining fields, and by Hammer et al. (2000) and Mallen-Ornelas et al. (1999) in the Canada-France Redshift Survey.

The faint blue subset of the DEIMOS sample has similar luminosities, SFRs and optical colors to the compact galaxies found in the Hubble Deep Field by Phillips et al. (1997), though none are “compact” (optical half-light radii $< 0''.5$.) This is a selection effect in our sample. Galaxies with half-light radii this small are classified as stars in SDSS and would not have been selected for spectroscopy in our sample. In Figure 11 we plot, as filled diamonds, the rest frame absolute B magnitude versus the B magnitude surface brightness and SFR versus velocity dispersion. The absolute B magnitudes are calculated from the observed bandpasses using the k-correction code of Blanton et al. (2003), and the surface brightness are calculated with the half-light SDSS r petrosian radii. The velocity dispersions are derived from the measured linewidths of [OIII]5007 for objects with $\geq 3\sigma$ detections of the emission line. For comparison, we also plot, as stars and squares, the faint blue galaxy samples of Koo et al (1995); Guzmán et al. (1996) and Phillips et al. (1997) making the necessary corrections to our adopted cosmology. While our sample of galaxies have luminosities, SFRs, and velocity dispersions comparable with the previous samples, the size selection effect separates our sample from the previous samples in surface brightness.

Koo et al (1995) and Guzmán et al. (1998) propose that the subset of the faint blue population of galaxies with compact geometry (half light radii $< 0''.5$) and narrow emission lines ($\sigma < 65 \text{ km s}^{-1}$) will fade to become dwarf spheroidals by $z=0$, while Hammer et al. (2000) claims that the most luminous of these are too massive to become dwarf spheroidals, and instead will become the bulges of spiral galaxies. The most massive intermediate redshift galaxies ($M_* \gtrsim 10^{10}$) in our sample could likely follow this latter evolution path. Indeed, we see that the galaxies in our sample that show extended structure at low redshifts ($z < 0.3$) are among the the most massive of the sample.

The conclusions of Koo et al (1995) and Guzmán et al. (1998) rest partially on the assumption that galactic winds from the last starburst event will remove the remaining gas from these systems and halt star formation causing them to fade several magnitudes by $z=0$. Through modeling the UV and optical broadband colors we find that about half the galaxies in our present sample could have formed at most $\sim 10\%$ of their stellar mass in bursts within the past 100 Myr, and only fifteen (all having $M_* < 10^9$) could have formed over 20% of their stellar mass within the last 100

Myr. If the last starburst event removes all remaining gas from these systems, as Koo et al (1995) propose, then why did the previous starforming events in these galaxies that produced the majority of the stars in these systems not halt star formation? Our derived starformation histories of these galaxies argues that the current star formation events will not halt starformation in every galaxy. But what percentage of these will continue to experience further bursts of star formation is unknown. However, even in the low mass systems of the present sample, residual star formation or another burst of star formation is ultimately unlikely to change the evolutionary outcome proposed by Koo et al (1995) and Guzmán et al. (1998) for the most compact low mass galaxies in our sample. We suggest that the more extended sources of our sample are more likely to become present-day dwarf irregulars rather than dwarf spheroidals.

7. SUMMARY

We have presented DEIMOS spectra for objects detected by *GALEX* in the MIS survey with imaged counterparts in SDSS; a total exposure time of 30 min per slitmask was used. *GALEX* has proven to be a sensitive instrument for wide field galaxy surveys. We have shown that the *GALEX* Medium Imaging Survey followed up with a 30 m integration with Keck/DEIMOS yields redshifts and line measurements for star forming galaxies to $z \sim 0.7$, and has yielded 4 QSO’s 3 of which are previously un cataloged. The matched sample reaches approximately 3 magnitudes fainter in r than the SDSS spectroscopic survey limits. The sample is not a homogeneous sample, but is indicative of the types of galaxies forming stars out to $z \sim 0.7$. We have derived physical parameters for these galaxies from the SEDS and compared this sample to a sample of 50,000 SDSS galaxies with *GALEX* detections.

1. We find that roughly one-third of the galaxies are starforming late type disk galaxies, four are QSOs at $z > 1$, and the remaining galaxies are faint blue low mass starbursts.

2. Approximately 3 out of 14 star forming galaxies show emission line ratios indicative of an AGN. A similar fraction was found by Sullivan et al. (2000) in their UV selected sample.

3. The masses of the galaxies are typically lower than what is found locally in the SDSS spectroscopic sample. The range of M_* for the DEIMOS sample spans from 10^8 to $10^{11} M_\odot$, whereas the median of the SDSS spectroscopic sample is $\sim 5 \times 10^{10}$.

4. The SFRs of the galaxies at $z > 0.25$ are roughly an order of magnitude greater than the SFRs for the galaxies at $z < 0.25$.

5. Besides three of the most massive, and reddest in $NUV - r$ color, the remaining galaxies show evidence of a starburst in the last 100 Myr, with $\log b \sim -0.1$. Fifteen of the galaxies in the lower mass range of the sample could have formed more than 20% of their stellar mass in bursts of star formation within the last 100 Myr.

6. Our sample has similar velocity dispersions, SFRs, and B luminosities to previous samples of faint blue galaxies, though the galaxies in our present study are 2 mag fainter in surface brightness.

GALEX is a NASA Small Explorer, launched in April 2003. We gratefully acknowledge NASA's support for construction, operation, and science analysis for the *GALEX* mission, developed in cooperation with the Centre National d'Etudes Spatiales of France and the Korean Ministry of Science and Technology.

The authors wish to recognize and acknowledge the very significant cultural role and reverence that the summit of Mauna Kea has always had within the indigenous Hawaiian community. We are most fortunate to have the opportunity to conduct observations from this mountain. The analysis pipeline used to reduce the DEIMOS data was developed at UC Berkeley with support from NSF grant AST-0071048.

The authors thank an anonymous referee for extremely helpful comments.

Facilities: GALEX, KECK:II(DEIMOS)

REFERENCES

- Abazajian, K. et al. 2004, *AJ*, 128, 502
 Baldwin, J. A., Phillips, M. M., & Terlevich, R. 1981, *PASP*, 93, 5
 Bertin, E., & Arnouts, S. 1996, *A&AS*, 117, 393
 Blanton, M. et al. 2003, *AJ*, 125, 2276
 Brinchmann, J., Charlot, S., White, S. D. M., Tremonti, C., Kauffmann, G., Heckman, T., & Brinkmann, J. 2004, *MNRAS*, 351, 1151
 Bruzual, G. & Charlot, S. 2003, *MNRAS*, 344, 1000
 Charlot, S. & Longhetti 2000, *MNRAS*, 323 887
 Charlot, S. & Fall, S. M. 2000, *ApJ* 539, 718
 Davis M. et al. in *Discoveries and Research Prospects from 6- to 10-Meter-Class Telescopes II*. Edited by Guhathakurta, Puragra. Proceedings of the SPIE, Volume 4834, pp. 161-172 (2003)
 Ellis, R., S. 1007, *ARAA*, 35, 389
 Faber, S. M., et al. 2003, *Proc. SPIE*, 4841, 1657
 Fukugita, M., Ichikawa, T., Gunn, J. E., Doi, M., Shimasaku, K., & Schneider, D. P. 1996, *AJ*, 111, 1748
 Guzmán, R., Koo, D. C., Faber, S. M., Illingworth, G. D., Takamiya, M., Kron, R. G., & Bershady, M. A. 1996, *ApJ*, 460, 5
 Guzmán et al. 1997, *Apj*, 489, 559
 Guzmán, R., Jangren, A., Koo, D. C., Bershady, M. A., & Simard, L. 1998 *ApJ* 495, 13
 Hammer, F., Gruel, N., Thuan, T. X., Flores, H., & Infante, L. 2000, *ApJ*, 550, 570
 Hogg, D. W., Finkbeiner, D. P., Schlegel, D. J., and Gunn, J. E. 2001, *AJ*, 122, 2129
 Kauffmann, F. et al. 2003, *MNRAS*, 341,33
 Kennicutt, R. C., *ARA&A*, 36, 189
 Kennicutt R. C., Bresolin, F. & Garnett, D. R. 2003, *ApJ*, 591, 801
 Kewley, L. J., Dopita, M. A., Sutherland, R. S., Heisler, C. A., & Trevena, J. 2001, *ApJ*, 556,121
 Kobulnicky, H. A. & Kewley, L. 2004, *ApJ*, 617, 240
 Koo, D. C., Guzmán, R., Faber, S. M., Illingworth, G. D., Bershady, M. A., Kron, R. G., & Takamiya, M. 1995, *ApJ*, 440, 49
 Martin, C. D. et al. 2005, *ApJ*, 619, 1
 Martin, C. D. et al. 2005, *ApJ*, 619, 59
 Milliard, B., Donas, J., Laget, M., Armand, C., Vuillemin, A. 1992 *A&A*, 257, 24
 Morrissey, P. et al. 2005, *ApJ* 619, 7
 Mallen-Ornelas, G., Lilly, S. J., Crampton, D., & Schade, D. 1999, *ApJ*, 518, 83
 Osterbrock, D. E. 1989, *Astrophysics of Gaseous Nebulae and Active Edmunds*, M. G., Blackwell, D. E., Chun, M. S., & Smith, G. 1979, *MNRAS*, 189, 95
 Phillips, A. C. et al. 1997, *ApJ*, 489, 543
 Pier, J. R., Munn, J. A., Hindsley, R. B., Hennessy, G. S., Kent, S. M., Lupton, R. H., and Ivezić, Z. 2003, 125, 1559
 Salim, S. et al. 2005, *ApJ*, 619, 39
 Salim, S. et al 2007, arXiv:0704.3611
 Scalo, J. M. 1986. *Fundam. Cosm. Phys.* 11:1-278
 Schiminovich, D. et al. 2005, *ApJ*, 619,47
 D.J. Schlegel, D.P. Finkbeiner, & M. Davis, *ApJ*, 500, 525 (20 June 1998)
 Smith, J. A. et al. 2002, *AJ*, 123, 2121
 Stoughton, C. et al. 2002, *AJ*, 123, 485
 Strauss, M. A. et al. 2002, *AJ*, 124, 181
 Sullivan, M., Treyer, M. A., Ellis, S. R., Bridges, T. J., Milliard, B., Donas, J. 2000, *MNRAS*, 312, 442
 Tremonti, C. A. et al. 2004, *ApJ*, 613, 898
 Treyer, M. A. et al. 2005, *ApJ*, 619, 15
 Wyder, T. K et al. 2005, *ApJ*, 619, 15
 Wyder, T. K. 2006, in preparation

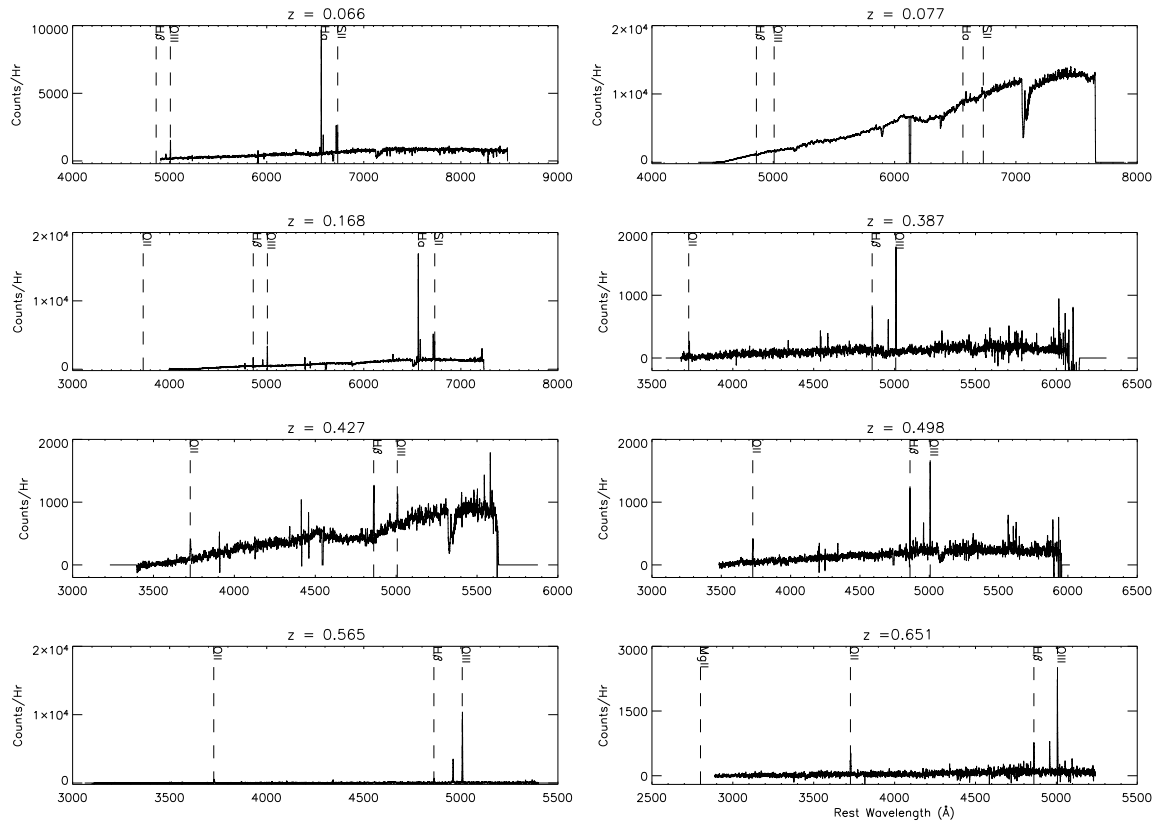


FIG. 1.— Spectra of several galaxies from our sample at a range of different redshifts. All of the galaxies are blue sequence galaxies except the galaxy at $z = 0.77$, which lies on the red sequence. The spectra have been boxcar smoothed by 5 pixels.

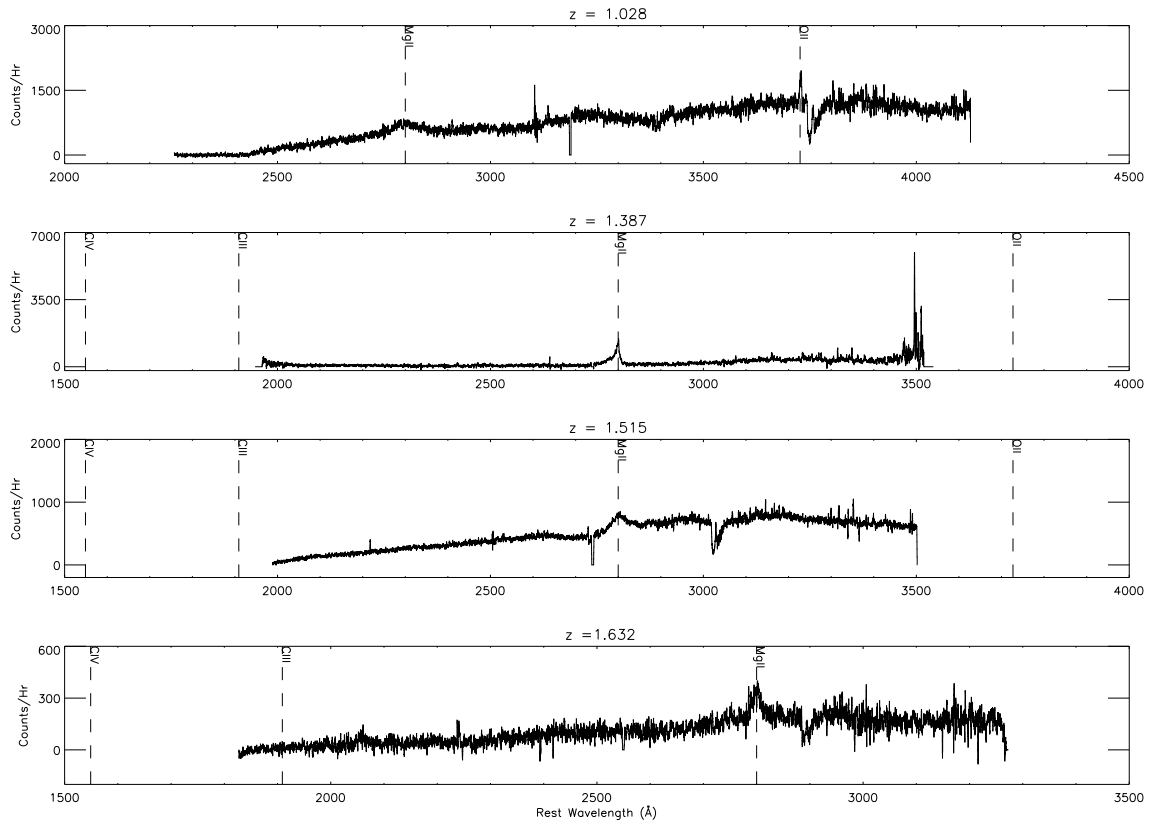


FIG. 2.— Spectra of four QSOs from our sample. The spectra have been smoothed by 5 pixels.

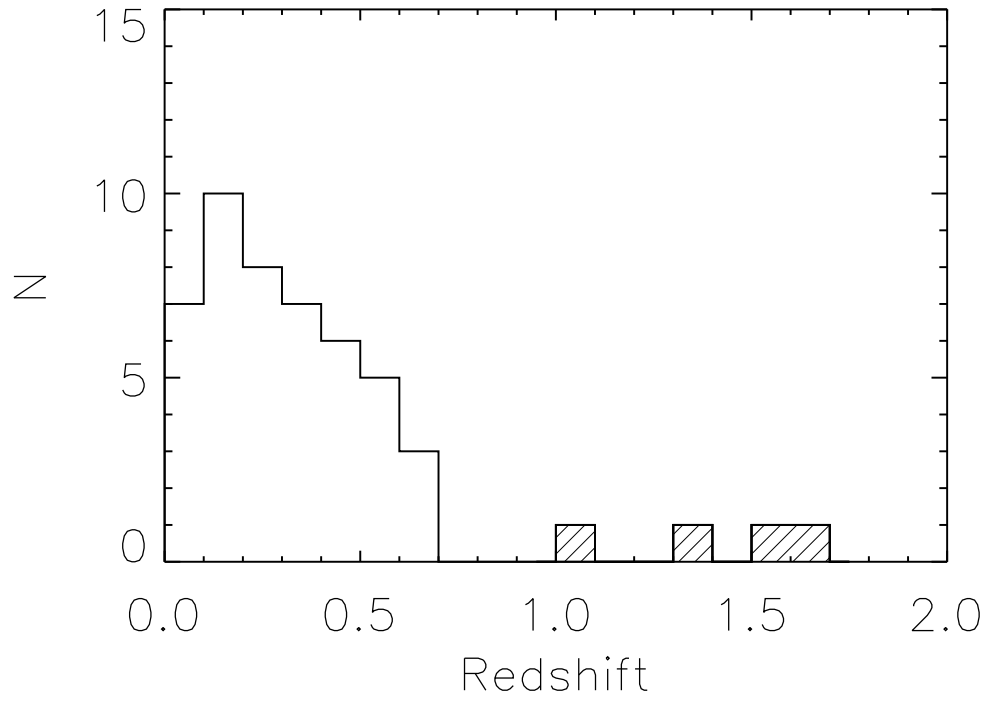


FIG. 3.— Redshift distribution of spectroscopic sample. The mean redshift for the sample is $z = 0.421$. Shaded boxes indicate the quasar redshifts.

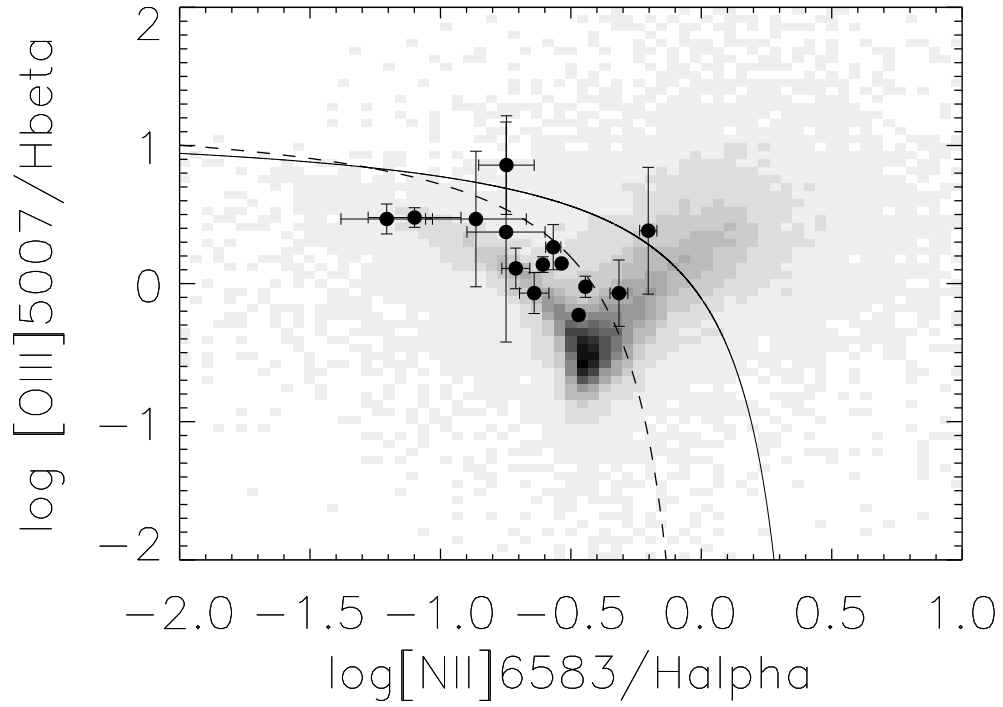


FIG. 4.— Emission line diagnostic diagram first used by Baldwin, Phillips, & Terlevich (1981). The shaded 2D-histogram corresponds to the GALEX IR1.1/SDSS DR2 spectroscopic sample. The dashed curves taken from Kewley et al. (2001); Kauffmann et al. (2003) show the distinction between sources with emission line flux coming from AGN (above) and sources with emission line flux coming from HII regions (below). Out of the 14 objects from our DEIMOS sample with detections of $H\beta$, [OIII], $H\alpha$, and [NII], only three have emission line ratios consistent with emission due to an AGN.

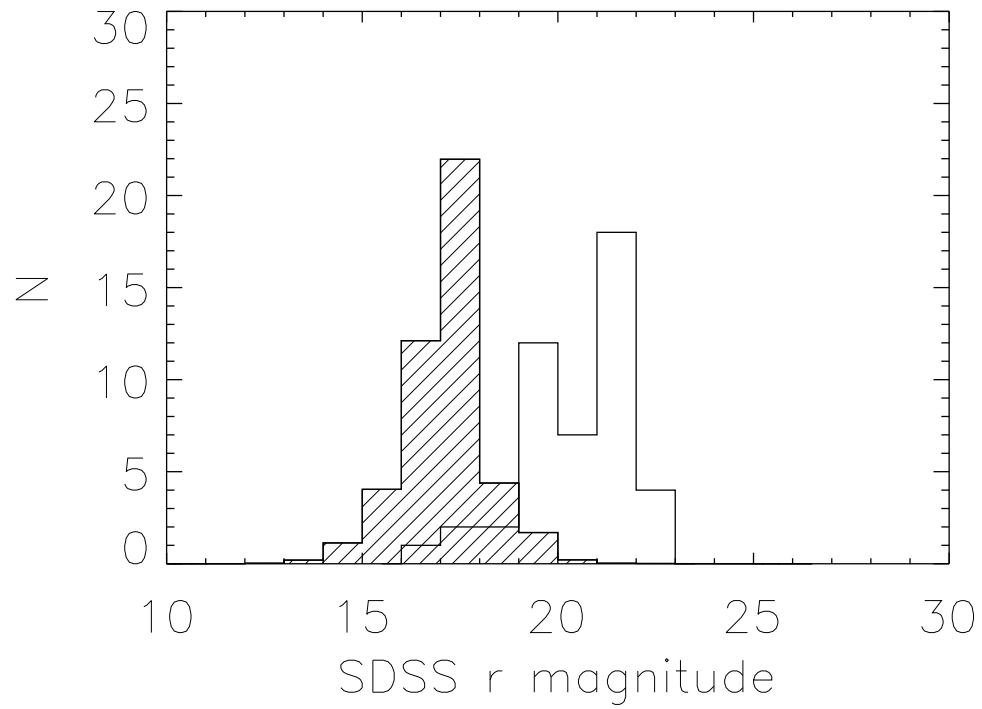


FIG. 5.— SDSS r magnitude distribution of the DEIMOS spectroscopic sample plotted with the SDSS r magnitude distribution of the matched GALEX IR1.1/SDSS DR2 spectroscopic sample (shaded histogram). The DEIMOS matched spectroscopic sample mean r magnitude (21) is 3 magnitudes fainter than the mean of the SDSS spectroscopic sample.

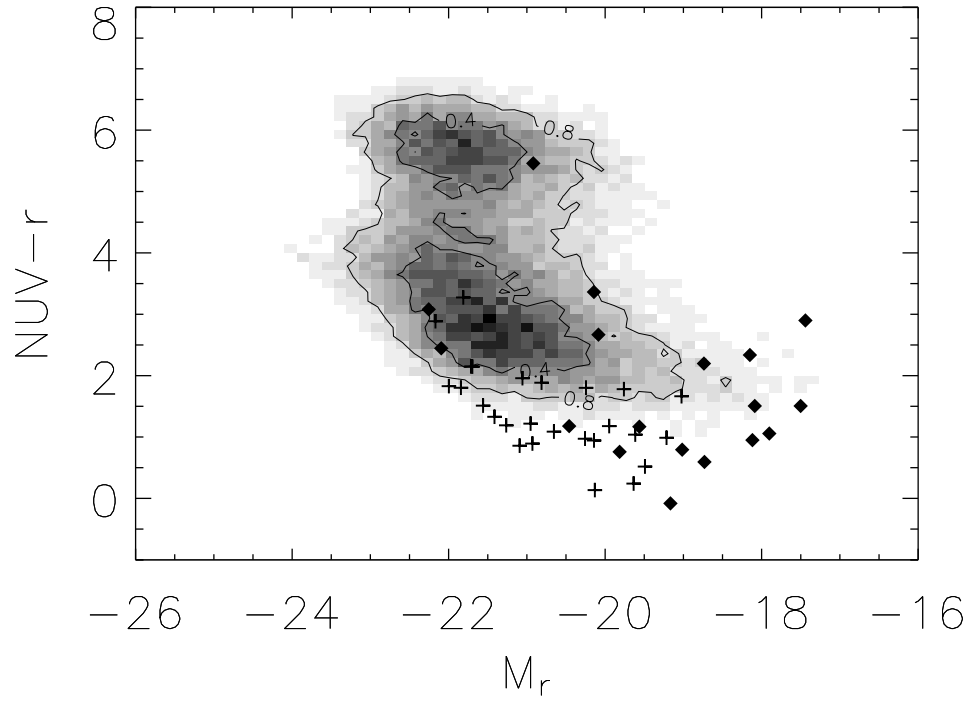


FIG. 6.— CMD of M_r vs. $NUV-r$ plotted for the sample of GALEX/SDSS objects with DEIMOS spectroscopy plotted with the entire GALEX(IR1.1)/SDSS (DR2) matched sample having SDSS spectroscopy. The diamonds represent galaxies in the DEIMOS sample at $z < 0.25$; crosses represent galaxies in the DEIMOS sample at $z > 0.25$. The IR1.1/DR2 sample is plotted as the shaded contour plot; the darker regions correspond to a higher density of points and the contours encompass 40% and 80% of the of the objects in the sample.

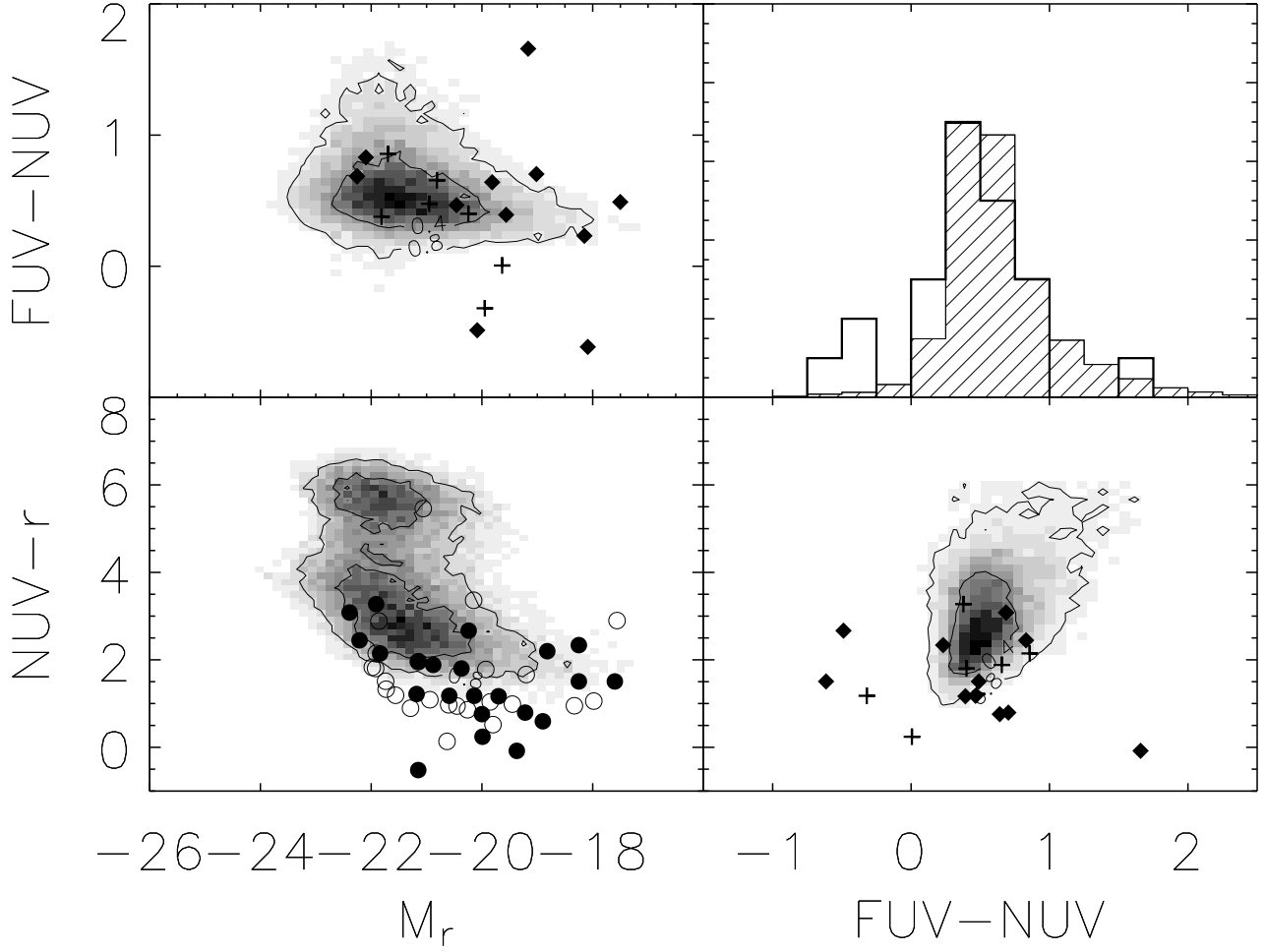


FIG. 7.— Panel 1: CMD of M_r vs. $FUV - NUV$ plotted for the 24 galaxies in the DEIMOS sample with FUV detections, plotted with objects in the IR1.1/DR2 matched sample with FUV detections shown as a shaded contour plot. PANEL 2: histogram of $FUV - NUV$ color for the 24 DEIMOS FUV galaxies plotted with distribution of the IR1.1/DR2 FUV sample (shaded histogram). PANEL 3: same as figure 5. The filled (unfilled) circles correspond to objects with (without) FUV detections. Panel 4: Color-Color diagram of the FUV DEIMOS galaxies again overplotted onto the FUV IR1.1/DEIMOS sample. The symbols used are the same as in figure 6 and the contours encompass 40% and 80% of the of the objects in the IR1.1/DR2 sample.

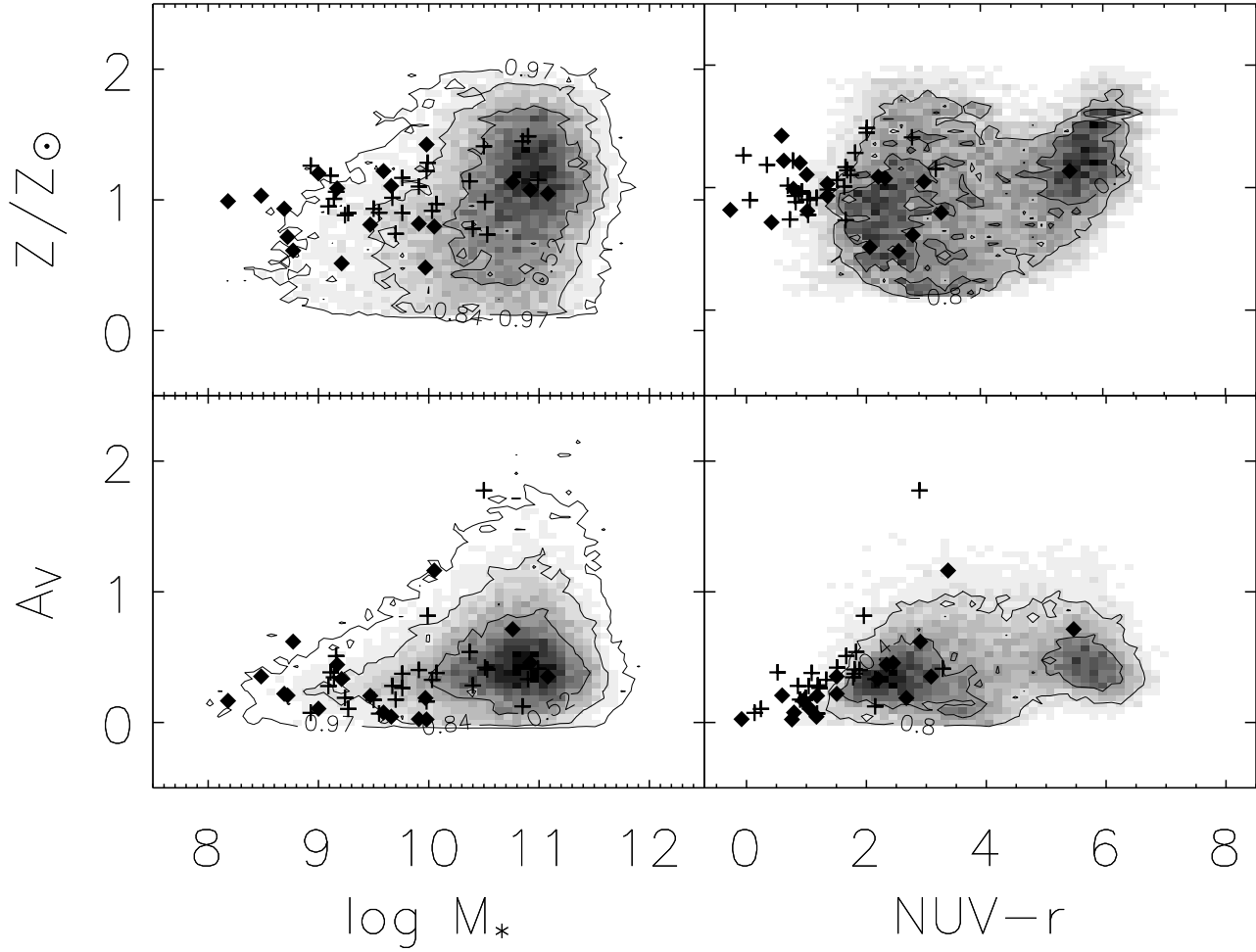


FIG. 8.— Derived Galaxy parameters, metallicity and V-band attenuation plotted versus M_* and $NUV - r$ color. The DEIMOS spectroscopic sample is plotted over the matched *GALEX* IR1.1/SDSS DR2 spectroscopic sample (shaded contour plot). The crosses correspond to objects with redshifts $z > 0.25$. The diamonds correspond to objects with redshifts $z < 0.25$. The contours for the plots of stellar mass contain 57%, 84%, and 97% of the data. The contours of $NUV - r$ color enclose 40% and 80% of the sample.

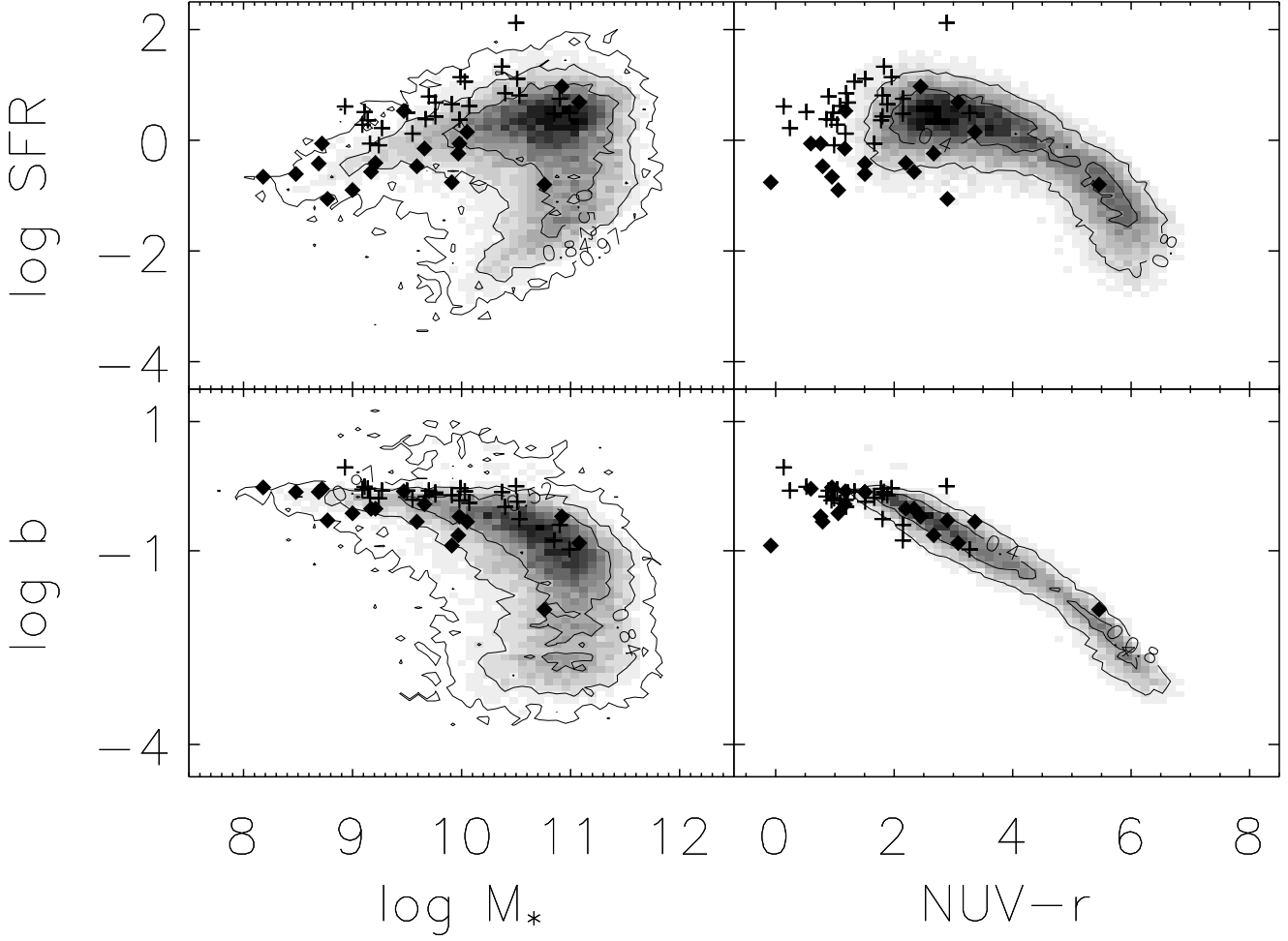


FIG. 9.— Derived Galaxy parameters, $\log \text{SFR}$ and $\log b$ plotted versus M_* and $NUV - r$ color. The DEIMOS spectroscopic sample is plotted over the matched *GALEX* IR1.1/SDSS DR2 spectroscopic sample (shaded contour plot). The crosses correspond to objects with redshifts $z > 0.25$. The diamonds correspond to objects with redshifts $z < 0.25$. The contours for the plots of M_* contain 56%, 84%, and 97% of the data. The contours of $NUV - r$ color enclose 40% and 80% of the data. The SFRs for the high z galaxies are approximately and order of magnitude higher than the SFRs of the low z galaxies.

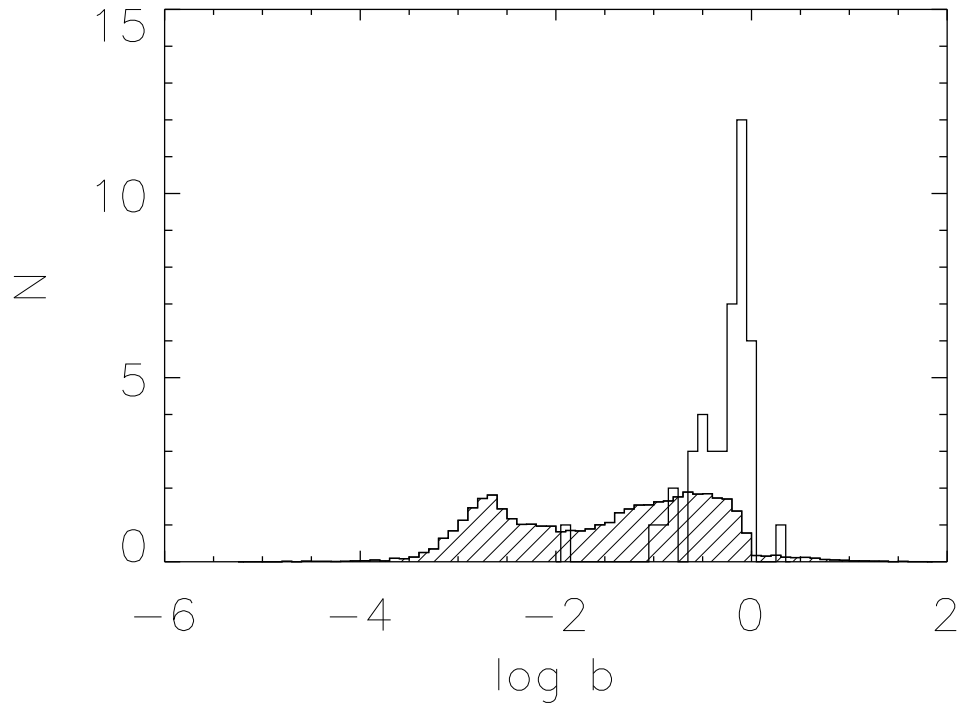


FIG. 10.— $\log b$ histogram distribution of the DEIMOS sample plotted with the $\log b$ distribution of the matched GALEX IR1.1/SDSS DR2 spectroscopic sample (shaded histogram) normalized to the size of the DEIMOS sample. This figure reflects our predominant sensitivity to the blue sequence star forming galaxies.

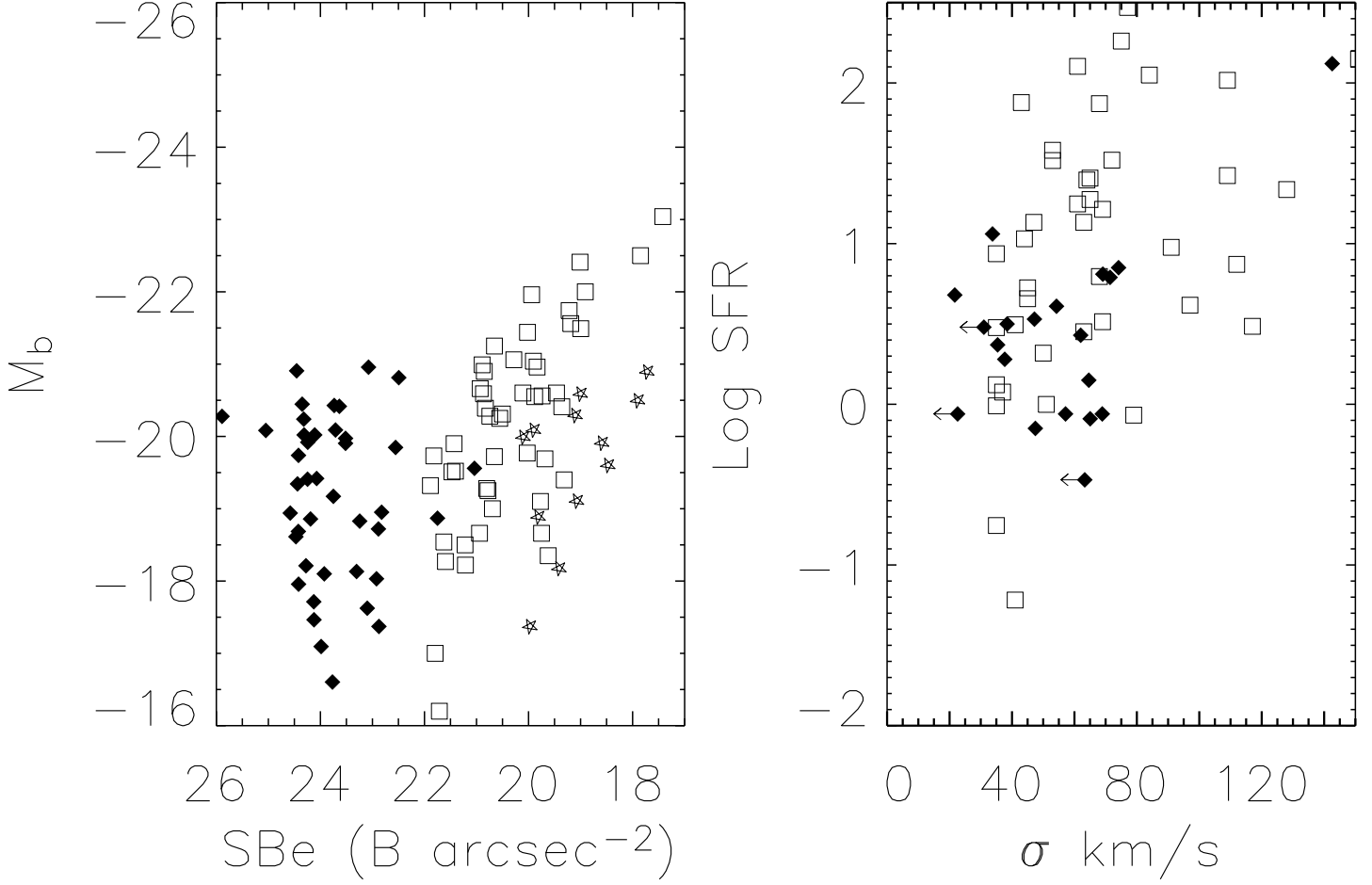


FIG. 11.— Panel 1: Rest frame absolute B magnitude, M_b , plotted versus the B-mag surface brightness within the petrosian r half-light radius. Panel 2: Star formation rate plotted versus measured velocity dispersions. The filled diamonds correspond to objects in our sample. Objects taken from Koo et al (1995) & Guzmán et al. (1996) are plotted as stars, and objects taken from Phillips et al. (1997) are plotted as squares. While the present sample has SFRs, luminosities, and velocity dispersions similar to the previous studies of faint blue galaxies, our sample contains sources with more extended emission and thus has lower surface brightness.

TABLE 1

SDSS Object ID	z	EW _{[OII]3727}	EW _{Hβ}	EW _{[OIII]5007}	EW _{Hα}	EW _{[NII]6584}	[OIII]5007/H β	[NII]6584/H α
587725578037494738	0.474	7.23 \pm 5.29	2.11 \pm 0.51	2.54 \pm 0.29	*** \pm ***	*** \pm ***	2.83 \pm 0.72	*** \pm ***
587725578037494286	0.134	*** \pm ***	2.05 \pm 0.20	2.57 \pm 0.22	4.51 \pm 0.05	3.46 \pm 0.13	1.37 \pm 0.18	0.25 \pm 0.01
587725591459201372	0.615	4.63 \pm 1.24	3.02 \pm 0.50	3.74 \pm 0.33	*** \pm ***	*** \pm ***	1.46 \pm 0.28	*** \pm ***
587725578037495014	0.213	*** \pm ***	6.16 \pm 4.88	4.83 \pm 4.78	58.32 \pm 30.70	3.91 \pm 16.30	1.12 \pm 1.38	0.98 \pm 0.60
587725578037494283	0.084	*** \pm ***	0.82 \pm 0.25	1.17 \pm 0.25	2.36 \pm 0.05	1.68 \pm 0.10	1.84 \pm 0.69	0.27 \pm 0.02
587725591459201726	0.439	5.21 \pm 0.35	3.17 \pm 0.18	3.34 \pm 0.06	*** \pm ***	*** \pm ***	4.95 \pm 0.30	*** \pm ***
587725591459201125 ^b	0.066	*** \pm ***	7.74 \pm 0.19	2.74 \pm 0.06	3.57 \pm 0.01	3.13 \pm 0.02	1.40 \pm 0.05	0.29 \pm 0.01
587725591459201562	0.068	*** \pm ***	0.81 \pm 0.82	1.51 \pm 0.75	2.66 \pm 0.19	1.17 \pm 0.51	2.93 \pm 3.32	0.14 \pm 0.06
587725591459201436	0.066	*** \pm ***	*** \pm ***	2.28 \pm 0.10	2.25 \pm 0.03	1.65 \pm 0.12	*** \pm ***	0.14 \pm 0.010
587725591459201670	0.651	6.22 \pm 0.58	3.66 \pm 0.77	5.06 \pm 0.21	*** \pm ***	*** \pm ***	3.98 \pm 0.84	*** \pm ***
587725591459201656	0.157	*** \pm ***	2.04 \pm 0.51	2.10 \pm 0.11	2.53 \pm 0.12	1.60 \pm 1.65	5.81 \pm 1.47	0.02 \pm 0.02
587725591459201666	0.078	*** \pm ***	1.03 \pm 1.80	1.08 \pm 0.62	2.10 \pm 0.11	1.50 \pm 0.51	2.36 \pm 4.33	0.18 \pm 0.06
587725591459201614	0.188	*** \pm ***	2.62 \pm 0.40	2.69 \pm 0.15	3.38 \pm 0.10	2.02 \pm 0.83	3.01 \pm 0.49	0.08 \pm 0.03
587725591459136404	0.220	*** \pm ***	0.74 \pm 0.59	3.43 \pm 0.57	4.95 \pm 0.23	2.77 \pm 0.67	7.21 \pm 5.93	0.18 \pm 0.04
587725591459136351	0.319	1.34 \pm 1.16	2.38 \pm 0.72	0.76 \pm 0.45	*** \pm ***	*** \pm ***	0.34 \pm 0.23	*** \pm ***
587725591459136031	0.192	*** \pm ***	0.25 \pm 0.22	0.59 \pm 0.34	2.98 \pm 0.12	2.79 \pm 0.18	2.42 \pm 2.55	0.63 \pm 0.05
587725591459136024 ^b	0.245	*** \pm ***	2.00 \pm 0.44	1.81 \pm 0.47	3.87 \pm 0.12	2.54 \pm 0.32	0.85 \pm 0.29	0.23 \pm 0.03
587725591459136330	0.565	8.01 \pm 0.95	3.13 \pm 0.32	3.43 \pm 0.11	*** \pm ***	*** \pm ***	18.69 \pm 1.78	*** \pm ***
587725591459135913	0.293	*** \pm ***	2.32 \pm 0.61	2.23 \pm 0.47	2.76 \pm 0.09	2.18 \pm 0.26	1.29 \pm 0.44	0.19 \pm 0.02
587725591459136277	0.290	*** \pm ***	*** \pm ***	1.81 \pm 1.07	0.82 \pm 0.44	2.80 \pm 0.41	*** \pm ***	3.97 \pm 2.21
587725591459136339	0.188	*** \pm ***	2.97 \pm 0.35	2.69 \pm 0.35	5.10 \pm 0.07	5.15 \pm 0.17	0.95 \pm 0.17	0.36 \pm 0.01
587725578037166749	0.320	*** \pm ***	2.30 \pm 0.35	2.45 \pm 0.86	*** \pm ***	*** \pm ***	0.59 \pm 0.22	*** \pm ***
587725578037166468	0.330	*** \pm ***	1.49 \pm 0.20	0.94 \pm 0.17	*** \pm ***	*** \pm ***	0.62 \pm 0.14	*** \pm ***
587725578037166557	0.168	*** \pm ***	2.47 \pm 0.11	3.06 \pm 0.07	4.11 \pm 0.03	3.06 \pm 0.09	2.39 \pm 0.12	0.20 \pm 0.01
587725578037166705	0.192	*** \pm ***	1.54 \pm 0.35	2.71 \pm 0.29	2.50 \pm 0.11	1.24 \pm 0.50	2.94 \pm 0.73	0.06 \pm 0.03
587725578037166672	0.189	*** \pm ***	3.85 \pm 0.15	2.92 \pm 0.20	5.48 \pm 0.03	5.96 \pm 0.07	0.59 \pm 0.05	0.34 \pm 0.01
587725578037166295	0.560	7.13 \pm 0.52	5.94 \pm 0.38	5.37 \pm 0.29	*** \pm ***	*** \pm ***	1.29 \pm 0.11	*** \pm ***
587725578037166628	0.652	0.95 \pm 0.65	3.54 \pm 0.43	0.86 \pm 0.45	*** \pm ***	*** \pm ***	0.17 \pm 0.09	*** \pm ***
587725578037166629	0.321	2.15 \pm 4.43	2.93 \pm 0.17	3.21 \pm 0.07	*** \pm ***	*** \pm ***	3.02 \pm 0.19	*** \pm ***
587725578037100839	0.561	5.25 \pm 0.34	2.84 \pm 0.15	4.40 \pm 0.25	*** \pm ***	*** \pm ***	1.70 \pm 0.13	*** \pm ***
587725578037101267	0.293	*** \pm ***	7.99 \pm 8.21	6.65 \pm 0.68	2.60 \pm 1.68	0.17 \pm 0.51	*** \pm ***	0.10 \pm 0.30
587725578037101221	0.518	5.79 \pm 0.95	3.31 \pm 0.35	*** \pm ***	*** \pm ***	*** \pm ***	*** \pm ***	*** \pm ***
587725578037100922	0.168	*** \pm ***	1.24 \pm 0.44	1.06 \pm 0.45	3.54 \pm 0.11	2.82 \pm 0.20	0.85 \pm 0.47	0.48 \pm 0.04
587725578037101176	0.281	*** \pm ***	2.28 \pm 0.29	3.52 \pm 0.27	2.49 \pm 0.08	*** \pm ***	2.07 \pm 0.31	*** \pm ***
587725591458873892	0.281	*** \pm ***	2.49 \pm 0.21	3.14 \pm 0.26	*** \pm ***	*** \pm ***	1.21 \pm 0.14	*** \pm ***
587725578037100775 ^a	0.176	*** \pm ***	*** \pm ***	*** \pm ***	0.86 \pm 0.11	1.07 \pm 0.08	*** \pm ***	1.30 \pm 0.20
587725591458808530	0.427	2.53 \pm 0.96	3.58 \pm 0.27	3.92 \pm 0.38	*** \pm ***	*** \pm ***	0.94 \pm 0.11	*** \pm ***
587725591458808528	0.598	5.42 \pm 0.31	3.57 \pm 0.20	*** \pm ***	*** \pm ***	*** \pm ***	*** \pm ***	*** \pm ***
587725578037101077	0.387	6.51 \pm 1.41	3.96 \pm 0.33	3.12 \pm 0.13	*** \pm ***	*** \pm ***	2.40 \pm 0.22	*** \pm ***
587725578037101473	0.496	4.81 \pm 1.31	2.44 \pm 0.52	2.95 \pm 0.13	*** \pm ***	*** \pm ***	4.70 \pm 1.01	*** \pm ***
587725578037166675	0.498	7.79 \pm 0.92	3.15 \pm 0.23	3.32 \pm 0.14	*** \pm ***	*** \pm ***	1.39 \pm 0.11	*** \pm ***

^a denotes objects with corresponding spectra in SDSS

^b denotes objects with failed SED fit

TABLE 2

SDSS Object ID	z	RA	Dec	FUV	NUV	$NUV - r$	$\log M_*$	$\log \text{SFR}$	$\log b$
587725578037166705	0.192	17 ^h 37 ^m 30.681 ^s	57° 20' 8.70''	22.53	23.11	1.51	8.69	-0.42	-0.09
587725578037166675	0.498	17 ^h 37 ^m 34.409 ^s	57° 21' 13.71''	***	22.62	0.97	9.50	0.50	-0.07
587725578037166672	0.189	17 ^h 37 ^m 39.053 ^s	57° 21' 30.10''	***	23.04	3.36	10.05	0.15	-0.55
587725578037166749	0.320	17 ^h 37 ^m 41.177 ^s	57° 18' 46.29''	22.87	22.12	1.88	9.91	0.65	-0.14
587725578037100839	0.561	17 ^h 37 ^m 43.542 ^s	57° 24' 5.51''	***	22.19	1.19	10.40	0.85	-0.32
587725578037166468	0.330	17 ^h 37 ^m 45.923 ^s	57° 19' 17.19''	22.38	21.50	2.15	10.85	0.48	-0.84
587725578037166557	0.168	17 ^h 37 ^m 58.250 ^s	57° 20' 16.80''	20.61	20.12	1.18	9.47	0.53	-0.08
587725578037166295	0.560	17 ^h 37 ^m 59.495 ^s	57° 23' 21.80''	***	22.16	0.89	9.70	0.79	-0.07
587725578037166628	0.652	17 ^h 38 ^m 2.622 ^s	57° 23' 26.99''	***	22.73	1.51	10.51	1.11	-0.24
587725578037166629	0.321	17 ^h 38 ^m 7.756 ^s	57° 23' 34.90''	***	22.32	1.04	9.09	0.28	-0.05
587725578037101267	0.293	17 ^h 38 ^m 22.192 ^s	57° 25' 2.82''	***	23.36	1.66	9.16	-0.06	-0.18
587725578037100922	0.168	17 ^h 38 ^m 23.628 ^s	57° 27' 56.42''	21.48	21.97	2.67	9.97	-0.24	-0.76
587725578037101473	0.496	17 ^h 38 ^m 27.876 ^s	57° 26' 33.90''	22.91	22.28	1.22	9.76	0.68	-0.10
587725578037101077	0.387	17 ^h 38 ^m 36.526 ^s	57° 30' 38.59''	***	22.32	0.52	9.11	0.51	-0.01
587725578037101221	0.518	17 ^h 38 ^m 37.317 ^s	57° 26' 53.92''	***	22.50	1.09	10.07	0.62	-0.26
587725578037100775 ^a	0.176	17 ^h 38 ^m 37.646 ^s	57° 29' 13.99''	21.03	20.34	3.08	11.08	0.69	-0.88
587725578037101176	0.281	17 ^h 38 ^m 41.873 ^s	57° 28' 9.30''	***	22.33	0.99	9.24	-0.09	-0.19
587725591458873892	0.281	17 ^h 38 ^m 48.259 ^s	57° 29' 10.40''	22.69	22.23	1.80	9.76	0.43	-0.13
587725591458808530	0.427	17 ^h 38 ^m 50.596 ^s	57° 29' 54.31''	***	22.88	2.89	10.50	2.12	0.00
587725591458808528	0.598	17 ^h 38 ^m 54.873 ^s	57° 30' 5.80''	***	22.58	1.83	10.37	1.33	-0.09
587725578037494286	0.134	17 ^h 39 ^m 45.205 ^s	56° 40' 2.20''	20.87	20.47	1.17	9.66	-0.15	-0.28
587725578037494409	0.355	17 ^h 39 ^m 51.035 ^s	56° 39' 13.11''	***	23.23	1.78	9.14	0.36	-0.04
587725578037495014	0.213	17 ^h 39 ^m 51.343 ^s	56° 39' 58.89''	***	22.73	0.95	8.18	-0.66	-0.02
587725578037494283	0.084	17 ^h 39 ^m 53.130 ^s	56° 40' 18.91''	22.24	22.00	2.34	9.17	-0.57	-0.35
587725578037494050	0.077	17 ^h 39 ^m 56.243 ^s	56° 38' 17.20''	***	22.11	5.46	10.76	-0.80	-1.91
587725578037494494	0.356	17 ^h 39 ^m 56.287 ^s	56° 37' 21.00''	***	22.20	1.96	9.99	1.14	-0.03
587725578037494738	0.474	17 ^h 39 ^m 56.704 ^s	56° 37' 53.80''	***	22.72	0.86	9.67	0.38	-0.16
587725591459201436	0.066	17 ^h 40 ^m 1.663 ^s	56° 44' 3.12''	20.89	20.74	2.20	9.21	-0.41	-0.35
587725591459201125 ^b	0.066	17 ^h 40 ^m 3.853 ^s	56° 41' 59.82''	20.37	19.99	1.96	***	***	***
587725591459201656	0.157	17 ^h 40 ^m 6.724 ^s	56° 43' 49.51''	22.64	22.12	-0.52	8.68	-0.97	-0.24
587725591459201627	0.079	17 ^h 40 ^m 8.196 ^s	56° 44' 57.80''	22.18	21.68	1.51	8.48	-0.61	-0.09
587725591459201372	0.615	17 ^h 40 ^m 8.328 ^s	56° 39' 39.82''	***	22.68	1.80	10.53	0.81	-0.51
587725591459201929	0.436	17 ^h 40 ^m 15.117 ^s	56° 46' 4.70''	22.36	22.16	0.24	9.27	0.22	-0.07
587725591459201726	0.439	17 ^h 40 ^m 17.307 ^s	56° 41' 31.09''	***	22.42	0.94	9.98	0.37	-0.22
587725591459136339	0.188	17 ^h 40 ^m 17.468 ^s	56° 48' 5.50''	21.23	20.57	0.76	9.98	-0.06	-0.47
587725591459201670	0.651	17 ^h 40 ^m 19.175 ^s	56° 43' 39.18''	***	22.46	0.14	8.93	0.61	0.29
587725591459201562	0.068	17 ^h 40 ^m 20.969 ^s	56° 42' 43.30''	***	22.77	2.90	8.77	-1.06	-0.53
587725591459201614	0.188	17 ^h 40 ^m 23.225 ^s	56° 45' 42.52''	22.37	21.50	0.59	8.72	-0.06	-0.04
587725591459136404	0.220	17 ^h 40 ^m 23.708 ^s	56° 46' 34.10''	22.53	21.76	0.79	9.59	-0.47	-0.55
587725591459135913	0.293	17 ^h 40 ^m 29.685 ^s	56° 50' 27.71''	21.64	21.93	1.18	9.55	0.12	-0.21
587725591459136024 ^b	0.245	17 ^h 40 ^m 32.498 ^s	56° 49' 12.51''	22.73	20.99	-0.08	***	***	***
587725591459201666	0.078	17 ^h 40 ^m 33.193 ^s	56° 44' 5.32''	***	20.82	1.06	9.00	-0.90	-0.42
587725591459136277	0.290	17 ^h 40 ^m 35.691 ^s	56° 50' 29.29''	22.66	22.23	3.27	10.99	0.49	-0.98
587725591459136330	0.565	17 ^h 40 ^m 46.362 ^s	56° 49' 13.40''	***	22.18	1.33	10.03	1.06	-0.08
587725591459136031	0.192	17 ^h 40 ^m 56.177 ^s	56° 49' 15.38''	20.94	20.09	2.45	10.92	0.97	-0.47
587725591459136351	0.319	17 ^h 40 ^m 56.594 ^s	56° 48' 52.20''	***	21.35	2.15	10.90	0.75	-0.60
587725578037100834	1.515	17 ^h 38 ^m 9.360 ^s	57° 25' 21.36''	***	23.40	2.63	***	***	***
587725591459201473	1.387	17 ^h 40 ^m 9.836 ^s	56° 40' 7.68''	***	22.67	1.14	***	***	***
587725591459136108	1.632	17 ^h 40 ^m 43.682 ^s	56° 48' 45.36''	***	23.05	1.67	***	***	***
587725591459135981 ^a	1.028	17 ^h 40 ^m 49.197 ^s	56° 47' 23.65''	22.62	21.20	1.94	***	***	***

^a denotes objects with corresponding spectra in SDSS^b denotes objects with failed SED fit